



THE UNIVERSITY OF
SYDNEY

SCHOOL OF AEROSPACE MECHANICAL AND MECHATRONIC ENGINEERING

AERO3760: SPACE ENGINEERING 2

Group E: SnapSat

Data Package Document 1 Critical Design Review

21 AUGUST 2015

Name and Email	Role and Responsibility
James Allworth 312073038 jall8741@uni.sydney.edu.au	<i>Attitude Determination and Control System</i> TASKS
Thomas Forbutt 312101058 tfor8012@uni.sydney.edu.au	<i>Communications and Data Handling</i> TASKS
Oscar McNulty 312106130 omcn3220@uni.sydney.edu.au	<i>Structural Design and Development</i> TASKS
Penelope Player 312106718 ppla7388@uni.sydney.edu.au	<i>On-board Computer and Power System</i> TASKS
Nikita Sardesai 312088205 nsar2497@uni.sydney.edu.au	<i>Thermal System Design and Payload</i> TASKS

Table 0.1: caption

Contents

1 System Overview	4
2 Payload Design	5
2.1 Integration	6
3 Structural Subsystem	7
4 Attitude Determination and Control Subsystem	8
4.1 Inertial Measurement Unit	8
4.2 Photodiode Sun Sensor System	8
5 Selection of Magnetorquers	8
6 Design of Magnetorquer	8
7 Construction of Magnetorquers	9
8 Magnetorquer Control System	11
9 Electrical Power Subsystem	12
9.1 Charging Circuit	12
9.2 Voltage Rails	12
9.3 Battery Lifetime	13
10 On-Board Computer and On-board Data Handling Subsystem	14
10.1 Selection	14
10.2 On-board Data Handling	14
10.3 Modes of Operation	15
11 Communications Subsystem	16
12 Thermal Control Subsystem	17
12.1 The Three Modes of Heat Transfer	17
12.1.1 Convection	18
12.1.2 Conduction	18
12.1.3 Radiation	18
12.2 Total Incoming Radiation	18
12.2.1 View Factors	19
12.3 Spacecraft Thermal Environment	20
12.3.1 Solar Radiation	20
12.3.2 Earth Infrared Radiation	21
12.3.3 Earth Albedo	21
12.3.4 Total Incoming Radiation Per Panel	22

List of Figures

2.1	An image of the ArduCAM Mini. Note that there is no storage mechanism on this module, necessitating an external SD card.	5
2.2	The SD card used in SnapSat	6
7.1	Magnetorquer Construction Set Up	10
7.2	Completed Magnetorquer	11
8.1	Simulink Model of Control System	11
9.1	The EPS PCB. Although this PCB is full it is functional, and the extra changing circuit has not taken the place of another component.	12
10.1	A diagram showing the interactions between the MCU and the other subsystems. .	14
10.2	A diagram showing the modes of operation during flight.	15
12.1	Incoming thermal radiation on the satellite	17
12.2	Radiation incoming onto the satellite as it orbits	19
12.3	Representation of Satellite Orbit	20
12.4	Solar radiation falling on each panel	21
12.5	Reflected albedo falling on each panel	22
12.6	Total radiation falling upon panel 2	22

List of Tables

0.1	caption	1
6.1	Predicted Data for the Magnetorquers	9

1 System Overview

The SnapSat is low budget (<\$1000) 1U CubeSat designed by University of Sydney students. Its purpose is to be launched 30km into the atmosphere on a weather balloon as a proof of concept for CubeSats.

It utilises a 3D printed chassis, tested blahblah structure stuff

Computationally, it consists of 5 major modules; the payload, attitude control and determination system (ADCS), location system, communications system.

2 Payload Design

The SnapSat payload is a single camera, used to take images of the earth throughout the flight. Due to the inherent size and power limitation of CubeSats, budget and ease of interface with the Iduino Due Pro, the 2MP ArduCAM Mini was selected.



Figure 2.1: An image of the ArduCAM Mini. Note that there is no storage mechanism on this module, necessitating an external SD card.

Unlike the ArduCAM, on which this is based, the ArduCAM mini has no integrated SD Card to store photos. As such, the design includes an Adafruit SD Card which stores all pictures.

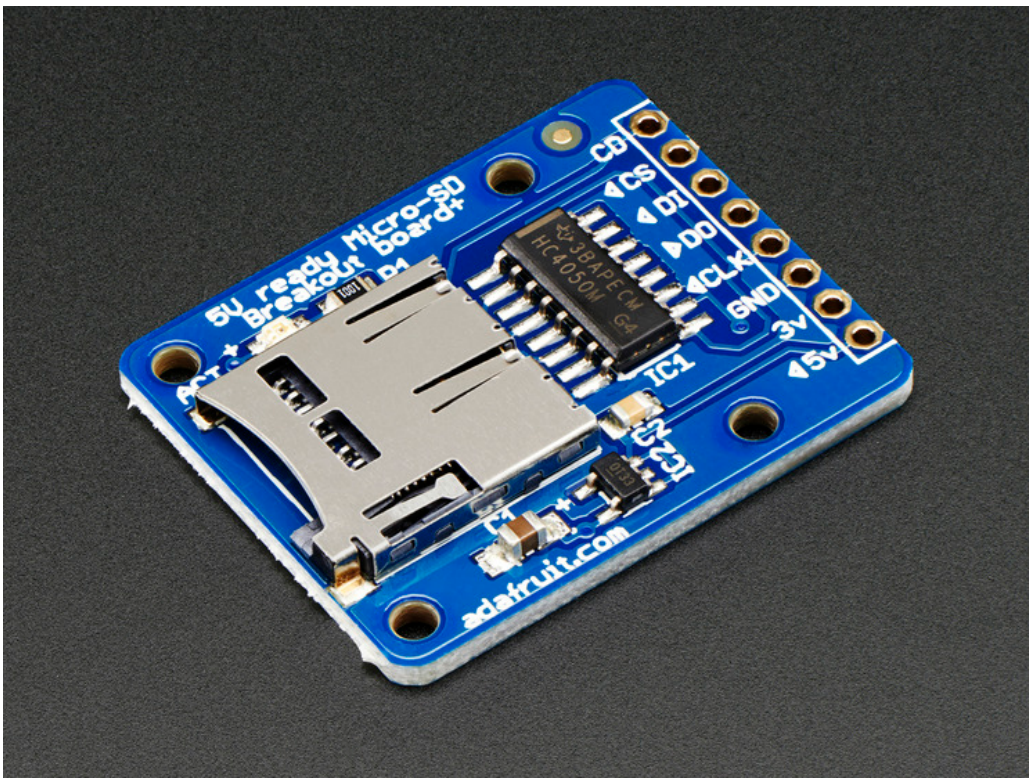


Figure 2.2: The SD card used in SnapSat

2.1 Integration

These two devices operate off the one SPI module and are physically located on the Bottom PCB. Additionally, the ArduCAM mini image sensor is controlled through I2C1 module. Both devices are powered by the 5V line, and use 3.3V CMOS logic levels, with no step up required.

STICK IN IMAGE OF BOTTOM PCB COMPLETED

Ultimately using a 16GB SD Card, assuming a size of 1MB per photo, and a balloon flight time of 4 hours this module is able to record 16000 photos or a photo every second.

3 Structural Subsystem

4 Attitude Determination and Control Subsystem

4.1 Inertial Measurement Unit

The inertial measurement unit (IMU) that was selected for the balloon launch is a 10 degree of freedom (DOF) Adafruit IMU. It includes a 3DOF magnetometer, a 3D0F accelerometer and a 3DOF gyroscope as well as a barometric pressure/altitude sensor which also includes temperature. The IMU uses an Attitude Heading and Reference System (AHRS) algorithm that returns the pitch, yaw and roll of the satellite with respect to magnetic north. Given the fact that this is a very cheap IMU there is a degree of drift associated with the gyroscope which causes inaccuracies. There is also an error associated with the accelerometer however it is less than the the drift caused by the gyroscope. As such the accelerometer has been used to determine the attitude both for the balloon launch and in the functional testing as the photodiode system will not be functional in either of these tests.

In terms of the application in space for this component, the major problem with this IMU is that it is not radiation hardened which will result in larger errors the longer it remains in orbit and will eventually cause it to stop working. Thus in the event of an actual space launch, this component would need to be replaced with a radiation and preferably more accurate component. The other major error that effects the IMU is accumulated error which is directly related to the amount of time spent in orbit. Although this may be reduced in higher quality IMU's it will always be an issue. Thus a secondary orientation system is required in order to determine the attitude of the SnapSat accurately.

4.2 Photodiode Sun Sensor System

A photodiode based sun sensor system was selected to be the secondary orientation system in order to recalibrate the IMU and to use in long duration missions. This system was primarily selected because it provides enough pointing accuracy for the purposes of this mission and is significantly cheaper than the alternatives of star trackers or actual sun sensors. The actual component that was selected is an OSRAM SFH203P Photodiode. Although these are simply off the shelf components, a cover glass can be placed over the photodiodes in order to protect them from UV radiation.

5 Selection of Magnetorquers

The SnapSat is a relatively small satellite with low mass and power considerations. After extensive literature review it was determined that given the mass and power consideration of the SnapSat, magnetorquers would provide a better controls system than

6 Design of Magnetorquer

The torque on the satellite produced by the magnetorquer is given by cross product of the magnetic dipole of the magnetorquer and the earths magnetic field strength:

$$T = M \times B$$

It is impossible to change the earth's magnetic field strength which is approximately 3×10^{-6} Tesla. Thus in order to maximise the torque on the satellite the magnetic dipole must be maximised. The magnetic dipole for the magnetorquer is given by the following equation:

$$M = N \cdot I \cdot A$$

Thus the magnetic dipole is dependent on the number of turns in the coil, the current through the wire and the area of the coil. Initially it seems like a simple problem where the dipole will simply increase with the number of turns if the current and area are held constant. However, this view does not take into account the resistance that increases with the length of wire, which given the fixed voltage will limit the current. Due to cost restrictions, only 0.18mm round copper wire was available for use, which had a resistance per metre (R_m) of 0.646 ohms. The following equations were then combined with the magnetic dipole equation in order to optimise the number of turns required:

$$I = \frac{V}{R}$$

$$R = N \cdot Perimeter \cdot R_m$$

$$P = V \cdot I$$

When combined the following equation was determined:

$$1 = \frac{4 \cdot M \cdot R_m}{V \cdot A}$$

Thus since resistance per metre and voltage are constant, and perimeter is dependent on area, the magnetic dipole becomes constant for a given area. Due to the restrictions in the lab only two sizes were available for the magnetorquers. The larger size was selected with side lengths of 0.073m as when the smaller size was modelled, the current draw was too high causing a higher level of power to be used. Thus given this fixed area, the maximum magnetic dipole was determined to be $0.14Am^2$. Using this maximum dipole as the basis, the other characteristics of the magnetorquer were determined and can be viewed in the table below.

Table 6.1: Predicted Data for the Magnetorquers

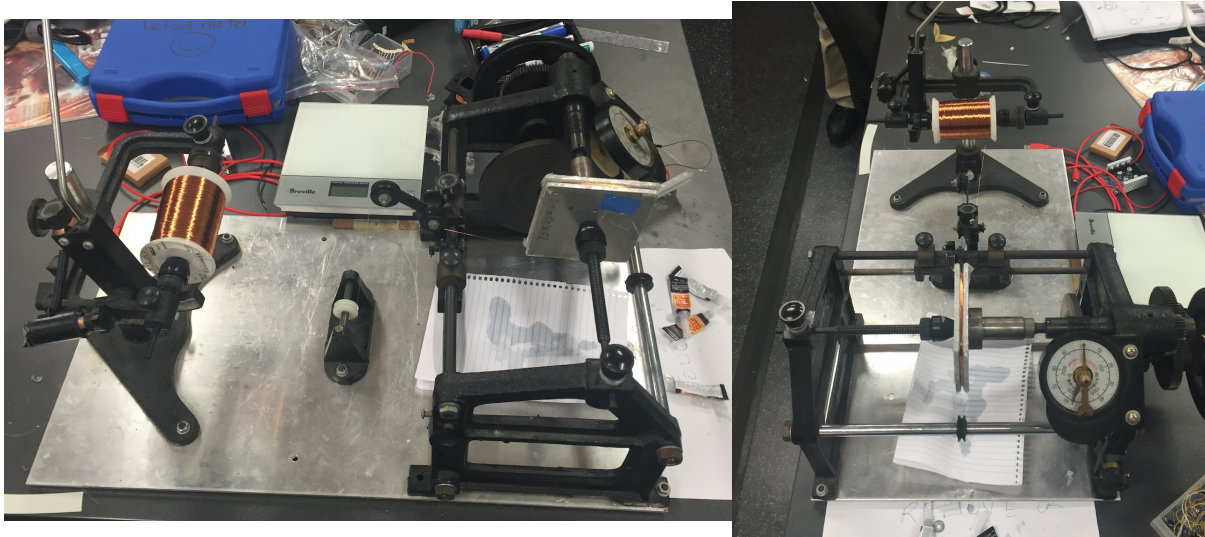
Magnetic Dipole	Number of Turns	Current	Area	Voltage	Resistance	Power Required
$0.14Am^2$	132	0.2A	$0.005329m^2$	5V	24.9Ω	1W

7 Construction of Magnetorquers

As mentioned previously the Magnetorquers were built in house using equipment provided in the space lab. The following procedure was applied to make each magnetorquer:

1. The metal structural mould for the magnetorquer was unscrewed and sticky tape was applied to areas that were likely to come into contact with glue.
2. The mould was placed in the winder and the copper wire was set up as shown in the photographs below.

Figure 7.1: Magnetorquer Construction Set Up



3. The wire at the very beginning of the coil was taped to the side of the mould to keep it separate from the coil so that it can be connected to the PCB.
4. In order to measure the number of turns, the counter on the winder was set to zero.
5. Twenty turns were completed and then a layer of super glue was added to the coiled wire on all four sides in order using a thin brush.
6. Step 4 was repeated until the required number of turns was reached at which point another layer of glue was added to each side of the coil.
7. The copper wire was cut and the wire at the very end of the coil was not stuck to the the main coil in order to provide a connection between the PCB and the magnetorquer.
8. The glue was allowed to set for 10 mins and then the coil was carefully removed from the mould with the aid of the sticky tape.
9. Once completed the ends of coil were carefully scraped with sandpaper in order to remove the protective coating and allow current to be passed through.
10. The coil was testing by attaching it to a battery and using a compass to determine whether a magnetic field was being produced.
11. An Ohmmeter was used to determine the resistance through the coil.

After testing both magnetorquers were found to have a slightly higher resistance than predicted with the first magnetorquer reading a resistance of 27.2Ω and the second magnetorquer reading 28.1Ω . This is roughly a 10% increase on the predicted value of 24.9Ω and is most likely caused by the effect of the super glue which was not taken into consideration in the original calculations. This will result in the magnetorquers using a slightly lower current as voltage is constant and have a lower maximum dipole value. These values were calculated to be 0.138Am^2 and 0.137Am^2 for magnetorquers 1 and 2 respectively. The image below depicts magnetorquer 1 just after construction.

Figure 7.2: Completed Magnetorquer



8 Magnetorquer Control System

The dynamic model for the magnetorquer control system was produced by three fundamental equations:

$$T = N \cdot I \cdot A \cdot B \cdot \sin(\theta)$$

$$V = I \cdot R$$

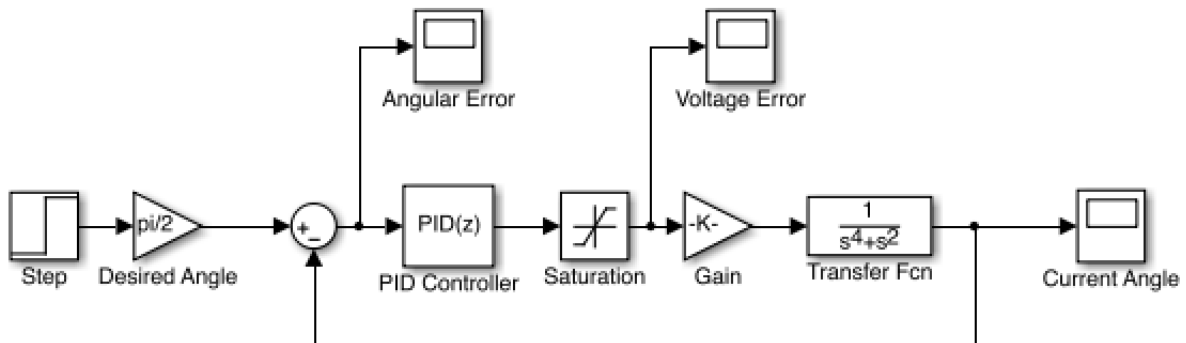
$$T = J \cdot \ddot{\theta}$$

By combining these three equations and using a Laplace transform the following dynamic model was determined:

$$\frac{\theta(s)}{V(s)} = \frac{N \cdot A \cdot B}{J \cdot R \cdot s^2(s^2 + 1)}$$

Thus using this function the following Simulink model was produced to determine the expected response of the satellite given certain inputs.

Figure 8.1: Simulink Model of Control System



9 Electrical Power Subsystem

The Electrical Power Subsystem (EPS) has the function of providing power to the CubeSat. For orbital flights power comes from 1W solar cells mounted on 5 of 6 faces, which charges the CubeSat at 1W when it is exposed to direct sunlight. However, for balloon flights there is insufficient incident light on the sides of the CubeSat due to the container in which it is mounted. As a result all power comes from two 1200mAh, 3.7 V Adafruit LiPo batteries mounted in the centre of the CubeSat.

FIGURE SHOWING LOCATION OF EPS BOARD

The EPS consists of two main sections; the charging circuit, and the voltage rails.

9.1 Charging Circuit

The charging circuit consists of two Adafruit LiPoly chargers designed to operate in conjunction with LiPo batteries and solar panels. They automatically draw off whichever source supplies the greatest amount of power (solar panels or batteries) which eliminates the need for a switching circuit when running off battery power. The only requirement is that the solar panels must provide a minimum of 6V output power supply to overcome the threshold of the internal circuit. By using two charging circuits rather than one, the batteries can be charged separately, which simplifies the load balancing at the expense of a fuller EPS PCB as shown in figure 9.1.

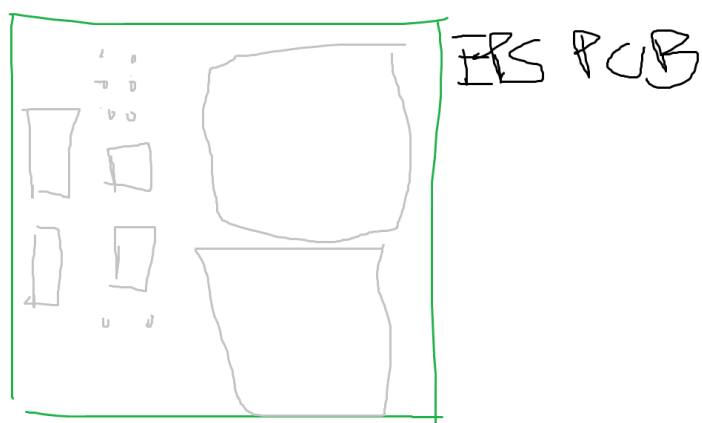


Figure 9.1: The EPS PCB. Although this PCB is full it is functional, and the extra charging circuit has not taken the place of another component.

9.2 Voltage Rails

Devices in this CubeSat require an even split of 3.3V and 5V power and some, the GPS in particular, require amperages above what the MCU can supply. Consequently, the EPS provides 3.3V and 5V power rails for components. However, although the MCU is a 3.3V device it is designed to run off an external supply of 6-20V, which is then transformed using an on board regulator into 5V and 3.3V. Given that, the EPS provides its own regulated 5V output which is fed directly into the Arduino's 5V

pin. This has the potential to damage the MCU if done incorrectly so the margin of error for the 5V rail is extremely small.

To transform the 3.7V battery power to 3.3V and 5V rails the system uses two TI Buck Boost converters, calibrated for 3.3V and 5V respectively. These are rated to a maximum current draw of 1.5A which is sufficient to power all devices and were chosen because of their reliability and output voltage stability [1].

9.3 Battery Lifetime

Given that the system operates using 250 mA CHECKCHECKCHECK(depending on the precise mode of operation) it can run for 10 hours off this configuration. As a standard balloon flight is expected to last for a maximum of 4 hours CHECKCHECKCHECK this is more than sufficient to power the CubeSat for the duration of the flight.

10 On-Board Computer and On-board Data Handling Subsystem

The SnapSat uses an Iduino Due Pro micro controller unit (MCU) to control it's operation. It does not use an RTOS, instead using the real time clock to trigger events at pre-set times and interrupt based control to prioritize incoming messages of the communications subsystem and other time critical systems (see figure

10.1 Selection

The Iduino Due Pro was chosen because it is a powerful micro controller, with a large amount of program space and sufficient peripherals to run all modules off. Additionally it has an external removable programmer, which gives it a relatively small form factor, (86.3mm by 53.3mm) allowing to fit easily within the CubeSat.

10.2 On-board Data Handling

The MCU interfaces with the other modules through the SPI, I2C1, I2C2, Serial0 and Serial3 peripherals, in addition to several GPIO pins as shown in figure 10.1. This leaves a Serial and NMEA module free which could easily be used to accommodate further subsystems in the future. Note that the SPI module and one of the I2C modules are shared between slave components, in such a way that more could be added to these busses in the future.

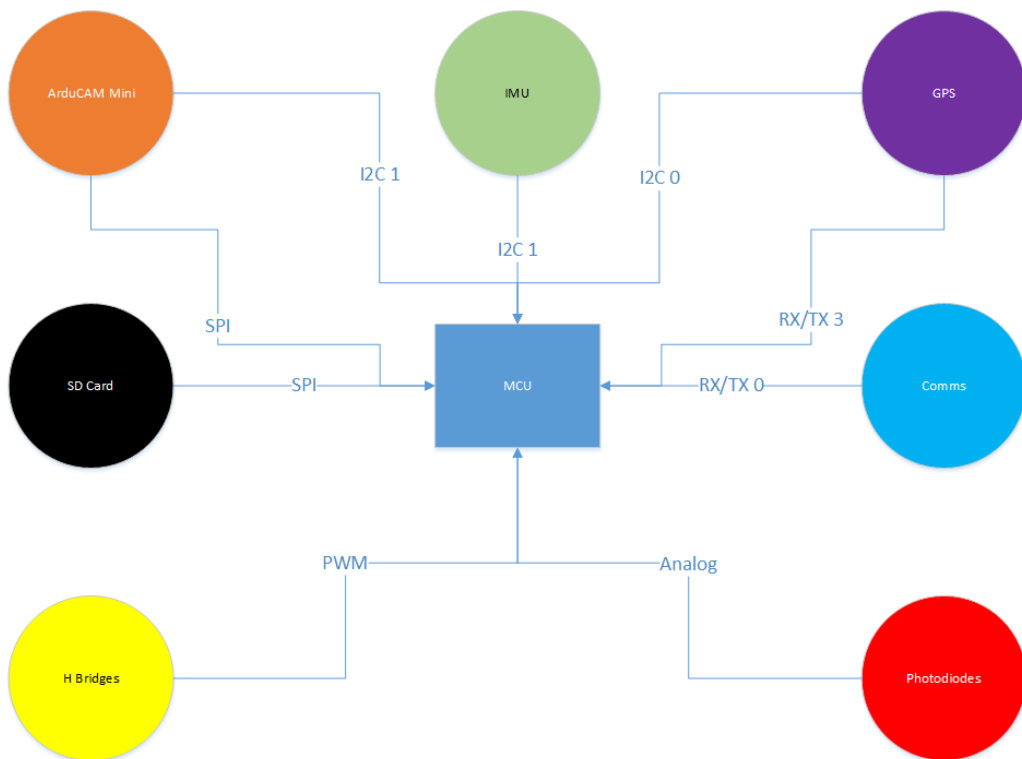


Figure 10.1: A diagram showing the interactions between the MCU and the other subsystems.

10.3 Modes of Operation

The CubeSat can operate in several modes of operation throughout an orbital flight, depending on the stage of flight, as laid out in the PDR and shown in figure 10.2.

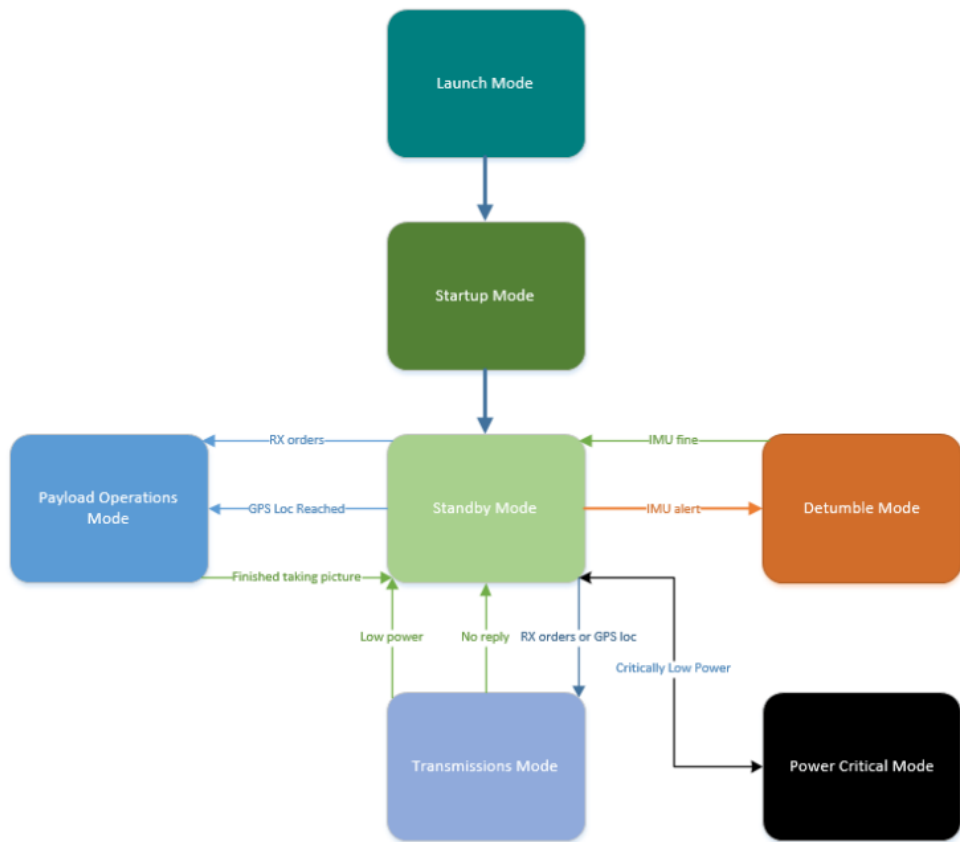


Figure 10.2: A diagram showing the modes of operation during flight.

Balloon flight, unlike orbital flights, have no CubeSat Design Specifications regarding power upon launch [2]. Consequently, SnapSat is to be launched in Standby mode while moving into Payload Operations Mode and Transmissions Mode as required. However, the CubeSat will never enter Power Critical Mode as shutting down extra systems to conserve power is ineffectual without operational solar panels or a similar means of charging.

11 Communications Subsystem

12 Thermal Control Subsystem

The method of developing thermal control used for SnapSat considers the following simplified model of the satellite. The main body is idealised as a system dissipating heat (located at the centre of the CubeSat) to the boundary located on the face of the CubeSat. This boundary is exposed to the outer environment. Energy conservation laws require that in steady state, the heat dissipated by the internal electronics is equal to that transferred to the boundary. Thus, the heat from internal dissipation added to the heat adsorbed from the outside is equal to the heat rejected to space. The general governing equation is

$$Q_{1 \rightarrow 2} = K_{1 \rightarrow 2}(T_a - T_2) \quad (12.1)$$

Where Q = heat exchange (Watts)

K = proportionality factor constant (Watts/Kelvin)

T = temperature of bodies (Kelvin)

between bodies 1 and 2. Additionally, the heat radiated from a blackbody surface of temperature T is given by

$$Q_r = KT^4 \quad (12.2)$$

Where the proportionality factor depends on physical constants, the material properties, surface conditions and geometry. A schematic of the incoming thermal radiation on the CubeSat in Low-Earth Orbit (LEO) is shown below.

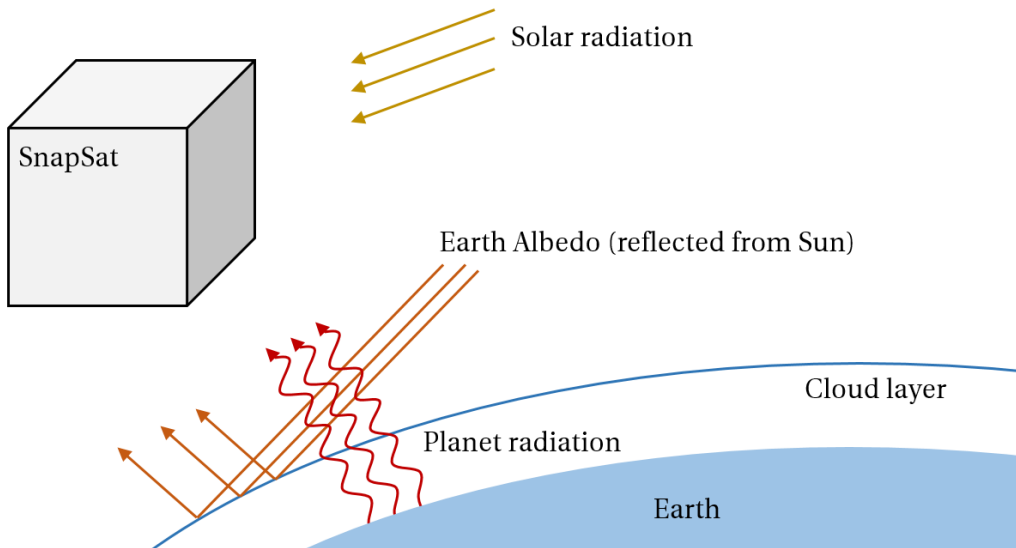


Figure 12.1: Incoming thermal radiation on the satellite

12.1 The Three Modes of Heat Transfer

The first law of thermodynamics states that the internal energy change on a system is equal to the amount of heat added subtracted by the amount of work done. The work done by the satellite on its environment is zero in our case, so the change in energy becomes

$$\frac{dU}{dt} = Q = A \rho c_p \frac{dT}{dt} dx$$

Where Q = heat added (Watts)
 A = cross-sectional area (m^2)
 ρ = density of material (kg/m^3)
 c_p = specific heat capacity ($\text{J}/\text{kg K}$)
 T = temperature (K)
 dx = incremental length (m)

Is is dependent on the physical and geometric properties of the satellite and the change in temperature. The total heat balance for the satellite is then given by the heat flux entering the system minus the flux leaving the system. These are characterised by the modes of heat transfer below.

12.1.1 Convection

Convection is the heat transfer between a solid surface and flowing fluid. This is of importance during mission launch, however does not apply in a space environment. Convection considerations were ignored for this design.

12.1.2 Conduction

Thermal energy transfer within a material due to vibrating atoms - for example if the material is heated in one location, conduction is the method by which it spreads to the rest of the material. This is most important for on-board electronics, the rate of heat transfer is given by

$$Q_{conduction} = \frac{kA}{\Delta x}(T_1 - T_2)$$

which is the same as equation 12.1. The heat transfer depends on the area of the satellite normal to the direction of heat transfer A , the thermal conductivity k and the temperature differential T .

12.1.3 Radiation

Perhaps the most complex form of heat transfer is radiation, where all bodies above 0K emit and absorb electromagnetic energy. We consider each body as a perfect emitter (black body) and integrate the emitted energy across all wavelengths, this gives

$$E_{bb} = \epsilon\sigma T^4 \quad (12.3)$$

measured in Watts/m^2 . This is the same as equation 12.2, where σ is the Stefan-Boltzmann constant. In this case, the emissivity ϵ has been added to account for the fact that the surfaces are not perfect black bodies.

12.2 Total Incoming Radiation

The total radiation incoming onto the satellite as it orbits is defined in figure 12.2 below. This assumes that the satellite is in full view of the sun 65% of the time in each orbit.

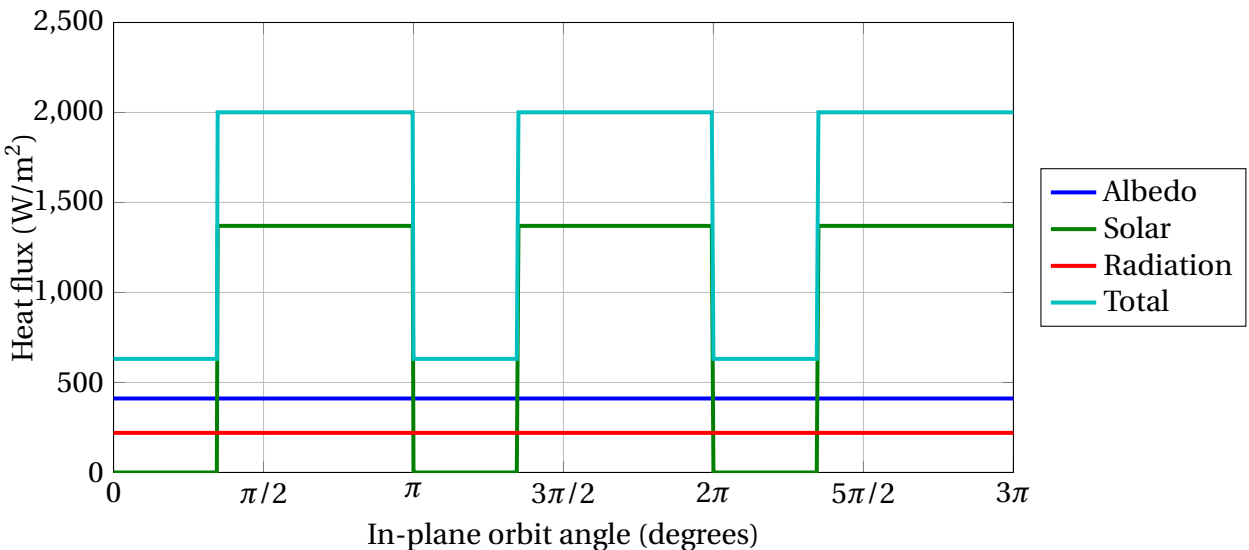


Figure 12.2: Radiation incoming onto the satellite as it orbits

Whilst this is the incoming radiation on the satellite as a whole, it is not indicative of the amount of radiation received by each side of the satellite. As the spacecraft is attitude controlled, the lower side will be facing the Earth always and only receive solar radiation for a short period of time. The amount of solar radiation (and even Earth IR radiation) received depends on the projected area that the radiation falls upon. Corrections are found using the view factor of each side of the satellite.

12.2.1 View Factors

The view factor of each side of the satellite allows for the calculation of the effect of the incoming radiation. The calculation takes into account the projected amount of heat flux on each side. The view factor is of importance when considering the radiation effect of Earth's infrared and albedo. The view factor indicates the area of the panel that radiation falls upon. The formulae to obtain the view factors for each panel is

$$F_{i \rightarrow j} = \frac{1}{A_i} \int_{A_i} \int_{A_j} \frac{\cos\theta_1 \cos\theta_j}{\pi S^2} \quad (12.4)$$

Where S is the shape factor. Whilst this a complex equation (especially for complex geometries), the view factors for a simple cubesat orbiting a sphere (Earth) are

$$V_F = \frac{\cos\gamma}{H} \quad (12.5)$$

If the panel is facing towards Earth such that the whole surface can be 'seen' by the panel. However if the panel is not facing the Earth

$$V_F = 0 \quad (12.6)$$

If the panel is oriented in such a way that it is only partially oriented to see the Earth then

$$V_F = \frac{1}{2} - \frac{1}{\pi} \sin^{-1} \left(\frac{(H^2 - 1)^{1/2}}{H \sin \gamma} \right) + \frac{1}{\pi H^2} \cos \gamma \cos^{-1} \left(-(H^2 - 1)^{1/2} \cot \gamma \right) \quad (12.7)$$

$$- \frac{1}{\pi H^2} (H^2 - 1)^{1/2} \times (1 - H^2 \cos^2 \gamma)^{1/2} \quad (12.8)$$

Where γ is the angle between the normal to the Earth's surface (or normal to the projected disk that the satellite panel sees) and the normal to the panel. [3]

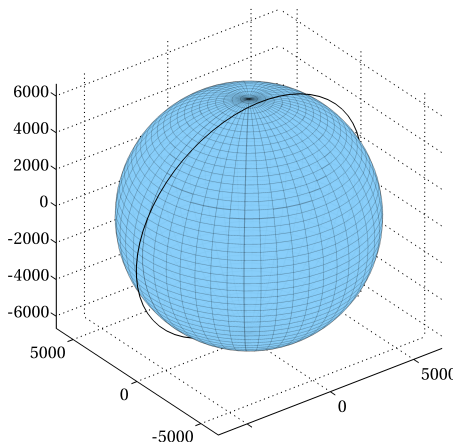


Figure 12.3: Representation of Satellite Orbit

12.3 Spacecraft Thermal Environment

As shown in figure 12.1, the spacecraft is subject to the following heating mediums: solar radiation, Earth infra-red and Earth albedo. The amount of radiation falling upon each panel is a function of the surface absorptivity and the view factor of the panel. The panel naming convention for this section is shown below.

12.3.1 Solar Radiation

The incoming solar radiation on the satellite is given by

$$Q_{solar} = Q_{sun} \alpha \cos \phi \quad (12.9)$$

Where $Q_{sun} = 1350$ solar heat flux (W/m^2)

α = panel surface absorptivity

ϕ = angle between the normal of the panel to the sun (rad)

For each of the panels, the solar radiation intensity is shown in the figure below. The skew in four of the panels is due to the 45° rotation of the orbit along the z Earth frame.

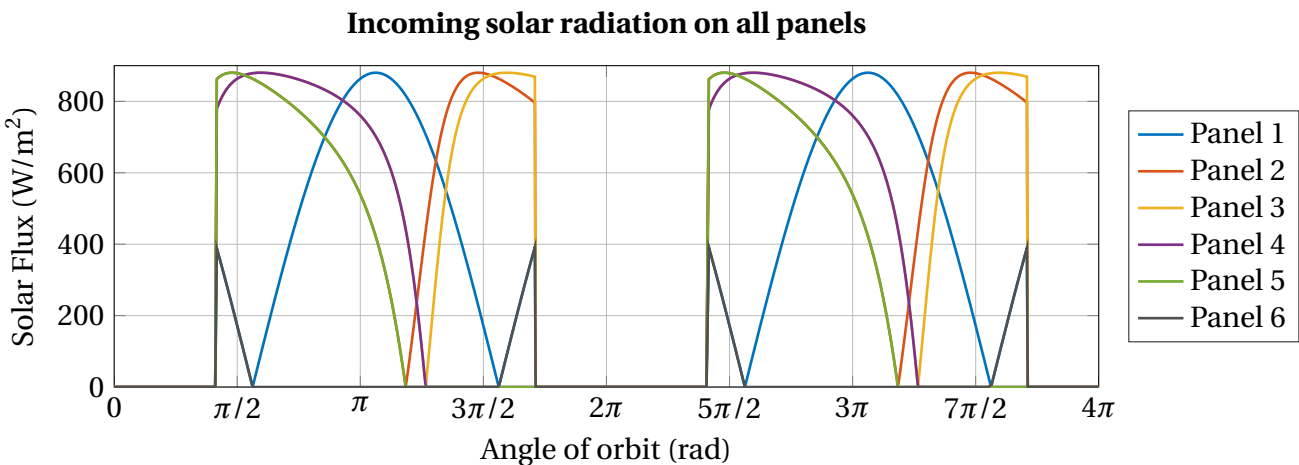


Figure 12.4: Solar radiation falling on each panel

12.3.2 Earth Infrared Radiation

The incoming radiation from the Earth is in the infrared band. This radiation is due to the effective temperature of the Earth and is a constant value for each panel. For this reason, the values will not be displayed on a graph. The incoming radiation varies from panel to panel depending only on the view factors as described in section 12.2.1. The value is given by

$$Q_{Earth-IR} = \sigma T_{Earth}^4 \alpha F_V \quad (12.10)$$

Where $\sigma = 1.381 \times 10^{-23} \text{ m}^2 \text{ kg s}^{-2} \text{ K}^{-4}$ (Boltmann constant)

T = effective temperature of the Earth

α = panel surface absorptivity

F_V = panel view factor

12.3.3 Earth Albedo

The final source of external radiation is the Earth albedo, which is solar radiation that has been reflected off the Earth's could layer. The value as the cubesat orbits the Earth is given by

$$Q_{Earth-albedo} = Q_{sun} F_A \alpha F_V \cos\theta \quad (12.11)$$

Where $Q_{sun} = 1350 \text{ W/m}^2$ (solar radiation)

F_A = albedo view factor

α = panel surface absorptivity

F_V = panel view factor

θ = angle between the spacecraft panel surface and the Sun

The figure below shows the variation in albedo that three panels see throughout the orbit. Since each panel is not double sided, the plot cycles between two opposite panels. For instance, the orange line shows the albedo incoming on both panels 2 and 5 (the panel on the opposite side). Half of the cycle representing each panel.

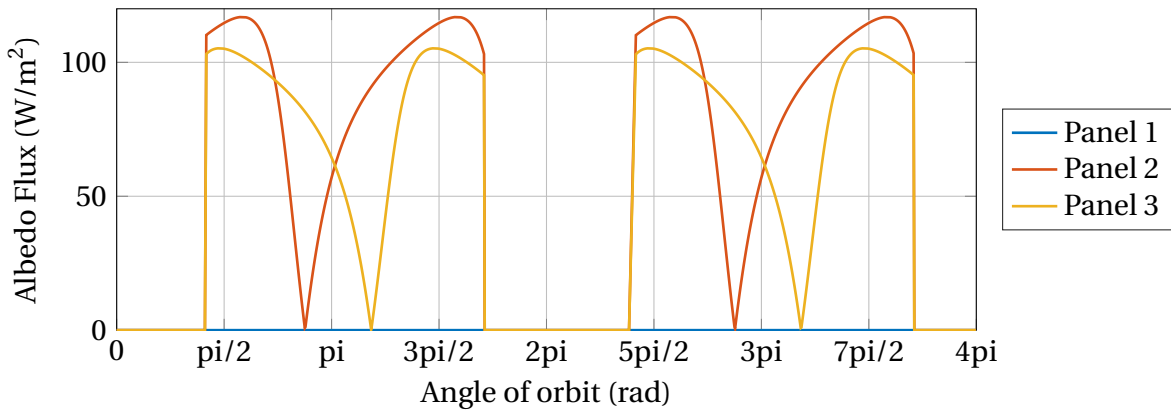


Figure 12.5: Reflected albedo falling on each panel

12.3.4 Total Incoming Radiation Per Panel

For illustration purposes, figure 12.6 shows the total incoming radiation on panel 2. This calculation was performed for all six panels.

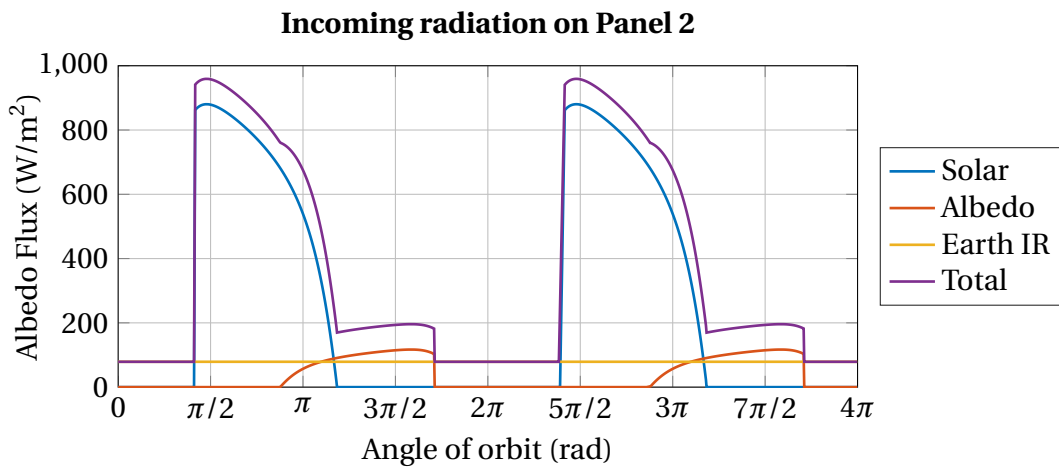


Figure 12.6: Total radiation falling upon panel 2

References

- [1] Texas Instruments, *1.5-A Peak Boost/Buck/Inverting Switching Regulators*, December 2004.
- [2] R. Munakata, “Cubesat design specification,” 2009.
- [3] H. Heidt, J. Puig-Suari, A. Moore, S. Nakasuka, and R. Twiggs, “Cubesat: A new generation of picosatellite for education and industry low-cost space experimentation,” 2000.